Al–Ce-Based Alloys: Processing, Mechanical Properties, and High-Temperature Stability

Humphrey Wara Odhiambo, Gaurav Singh, Mohamad Tasneem, Monica A. Soare, Jason Leszczewicz, Jun Cui, Ralph E. Napolitano, Gaoyuan Ouyang, and Catalin R. Picu

Abstract

A new generation of Al alloys based on the Al–Ce system, with microstructure and properties weakly sensitive to elevated temperatures, is being developed for applications such as thermal engine blocks and supersonic aircraft fuselage components, where high-performance calls for mechanical property retention during prolonged exposure to elevated temperature. Cast Al–Ce binary alloys with 10 and 16% Ce were produced by slab and book mold casting and their mechanical properties were measured and compared. Slab cast samples were further processed by extrusion, which increased strength and ductility by a factor of two. The as-cast and extruded Al–10%Ce showed 99% strength retention after long-term (100 h) exposure to 300 °C, with shorter-duration exposure (10 h) providing a 7% increase in strength. The microstructure and hardness did not change upon longer annealing times (up to 400 h), which indicates the outstanding thermal stability of this class of Al alloys. The microstructure of extruded samples observed using EBSD was modeled to determine the effect of the stiffness mismatch between $Al_{11}Ce_3$ precipitates and the Al matrix on the strain distribution. It was concluded that the mismatch effect is weak enough for the strain distribution in the two-phase alloy to be indistinguishable from that in the single-phase alloy. Therefore, the elastic contrast is expected to have little effect on the plastic deformation and fatigue response of these alloys.

Keywords

Al–Ce alloy • Mechanical properties • Processing

Introduction

Al alloys are broadly used in subsonic aircraft design due to their high specific strength and corrosion resistance. Supersonic aircrafts are subjected to elevated temperatures due to aerodynamic friction. The temperature of critical components of the skin and fuselage increases with the Mach number and reaches values of 300 °C at Mach 3 and larger than 450 °C at Mach 4. This precludes the use of conventional high-strength wrought Al alloys, such as the precipitation-hardened AA2XXX and AA7XXX series, as their properties degrade rapidly above ~220 °C [1]. With the primary strengthening mechanism of precipitation hardening being disabled at higher temperatures due to rapid precipitate coarsening and dissolution, design solutions frequently call for more thermally stable but heavier alloys, e.g. Ti-based, for such applications.

A new generation of temperature-resistant Al alloys based on the Al–Ce system is considered as a potential solution for high-temperature applications [2–7]. This is expected to replace some of the components currently made from Ti with much lighter Al, with subsequent weight savings that reflect in reduced energy consumption and reduced emissions. The goal of this material development effort is to obtain microstructures stable enough at the application temperature.

Ce is the most abundant rare earth metal, at present lacking high-volume applications. In the literature, it is described as one of the potential candidates for acting as a

H. W. Odhiambo · J. Cui · R. E. Napolitano · G. Ouyang (✉)
Department of Materials Science & Engineering, Iowa State University, Ames, IA 50011, USA
e-mail: gaoyuan@iastate.edu

G. Singh · M. Tasneem · C. R. Picu (✉)
Department of Mechanical, Aerospace, and Nuclear Engineering, RPI, Troy, NY 12180, USA
e-mail: picuc@rpi.edu

M. A. Soare · J. Leszczewicz
GE Aerospace Research, Niskayuna, NY 12309, USA

J. Cui · G. Ouyang
Division of Materials Sciences and Engineering, Ames National Laboratory, Ames, IA 50011, USA

L. Edwards (ed.), *Light Metals 2025*, The Minerals, Metals & Materials Series,
https://doi.org/10.1007/978-3-031-80676-6_10

primary alloying element in Al alloys [8, 9]. Ce has one of the lowest values of diffusivity and solubility in Al, which severely retards precipitate coarsening and promotes microstructural stability at elevated temperatures [2, 10–12].

Controlling the precipitate size is essential for strengthening, with a fine dispersion of precipitates being desirable. Cast Al–Ce alloys exhibit uneven spatial distribution of large precipitates, which does not lead to efficient strengthening [13, 14]. Al–Ce alloys exhibit improved castability compared with conventional wrought Al alloys and are not susceptible to hot tearing and cracking [15]. Given the promise of enhanced high-temperature performance, there is great interest in identifying effective methods for microstructural refinement of cast Al–Ce alloys to enhance their overall performance and broaden their applications.

Forging, rolling, and extrusion, as well as severe plastic deformation (SPD) processes, have been used extensively to produce microstructural refinement in metallic materials, however, processing of Al–Ce alloys by these methods has received little attention. Zhang et al. studied the effect of cold rolling and annealing on the mechanical properties for Al–9Ce alloy. The strength of the alloy increased, and load transfer was facilitated by oriented precipitation [16]. Stanislav et al. showed the effect of high-pressure torsion on the microstructure and tensile properties of Al–9Ce. The process leads to the formation of nanograins and a large increase in the yield stress and tensile strength [17, 18]. No reports are available in the literature on the effect of extrusion on microstructures and mechanical properties of Al–10Ce alloys.

The present work focuses on the processing of cast Al–10Ce and Al–16Ce and extruded Al–10Ce and Al–16Ce alloy (all percentages in wt%). Microstructures are characterized using SEM, XRD, and mechanical properties are measured at ambient temperature by uniaxial tensile testing and Vickers microhardness measurements. We examine the effect of casting methods for Al–10Ce alloys before and after heat treatment. The microstructural and mechanical properties characterization is performed on longer annealed time (200, 300, and 400 h.) for extruded Al–10Ce.

Experimental

Materials and Processing

Two types of casting were considered: book mold and slab casting, as shown in Fig. 1. Figure 1a, b show the two casting units with 200 and 2000 g capacity, respectively. The steel book mold (vertical cast) and the slab produced are shown in Fig. 1c, d. Figure 1e, f show the slab cast mold and resulting slab, respectively. The casting temperature is 800 °C for both casting methods. The mold is kept at room temperature for book mold casting and at 400 °C for slab casting.

The eutectic composition, Al–10Ce, and a hyper-eutectic composition, Al–16Ce, were selected for extrusion. 25.4 mm diameter as-cast rods were reduced to 9.5 mm diameter by extrusion at 300 °C using an Innovare LMS extrusion press. The extrusion furnace chamber is heated at a rate of 10 °C/min and samples are equilibrated at the target temperature for 30 min. Extrusion is performed by adjusting the pressure from 11.6 ksi (80 MPa) to 81.4 ksi (561 MPa) within 5 min. At the end of extrusion, a fan is used to cool the extruded rod to room temperature, after which the rod is ejected.

Tensile Test

Tensile specimens with 52 mm gauge length were machined using CNC per the ASTM E8 standard [19] for all cast, extruded, and heat-treated conditions. Tensile tests were performed using an Instron machine (Instron 5969, 50 kN load cell) under quasi-static conditions ($\dot{\varepsilon} = 3 \times 10^{-3} s^{-1}$) at room temperature (25 °C). Tests at elevated temperatures of 150, 200, 250, 300, and 350 °C were performed with the same system, the sample being heated at a rate of 5 $^{\circ}C/s$ to reach the test temperature, followed by a 300 s hold before the beginning of the test.

Hardness was measured with a microhardness tester (Qness 60M QATM) with a load of 500 g, with 15 s dwell time [20], in accordance with ASTM E92. At least three samples were tested in each condition, with 10 measurements per sample. The average values are reported here.

Microstructure Characterization

Test specimens for both XRD and metallographic (SEM) analysis were prepared by sectioning and grinding with fixed abrasive papers (320, 800, and 1200 grit) followed by polishing with loose abrasive suspension-embedded cloths (alumina and colloidal silica, 5–0.05 mm). XRD patterns were collected using a Panalytical XRD instrument with Cu–K_{α} radiation between 20 and 90°, with a scan rate of 1°/min. FEI SEM was used for the metallography and fractography studies. Polished planar surfaces were prepared for examination by etching with Kellar's reagent for 10 s whilst fracture surfaces were examined directly, with no further preparation.

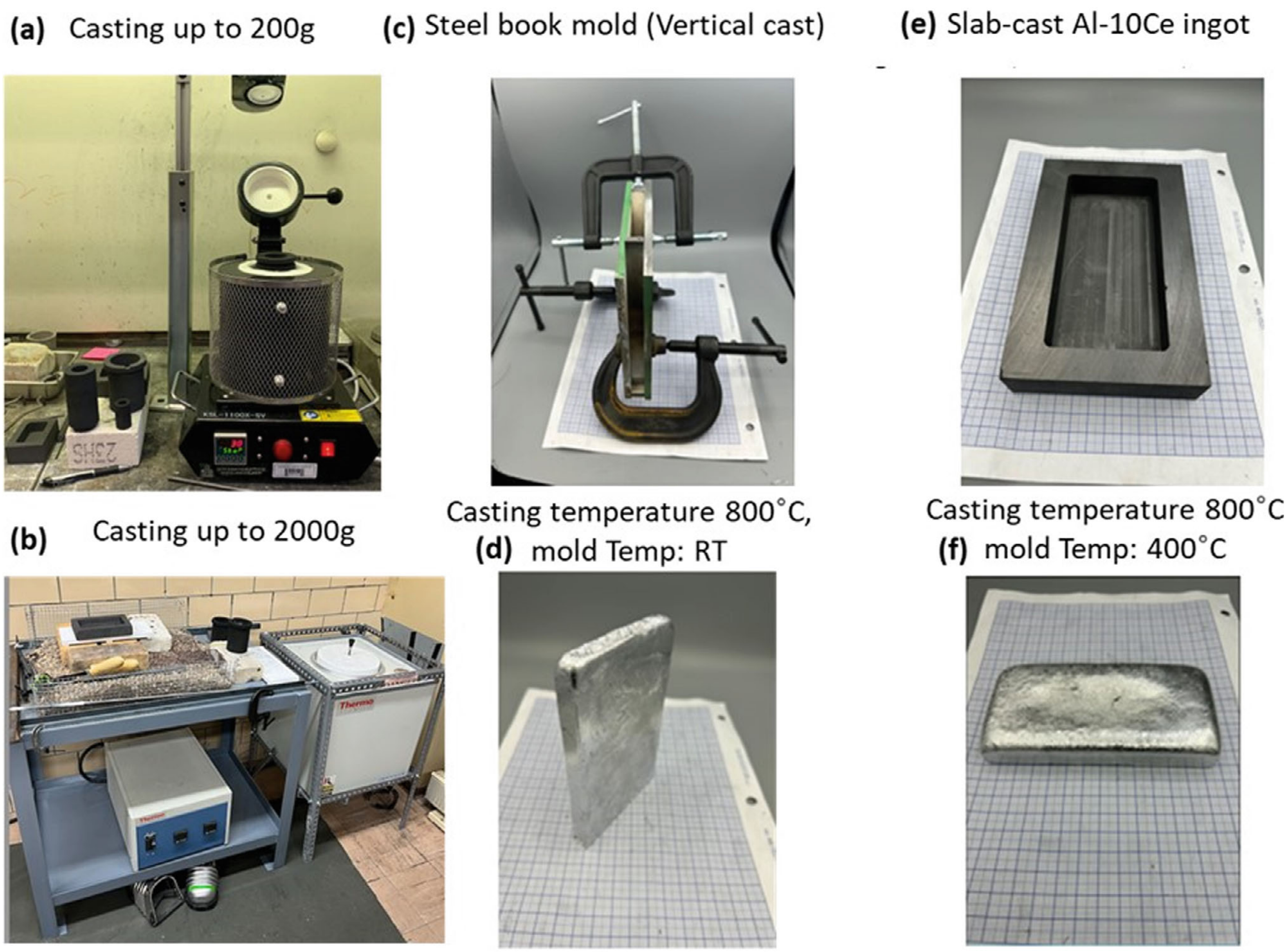

Fig. 1 Casting devices used for **a** samples up to 200 g and **b** samples up to 2000 g. Two different mold geometries have been used in the present work: **c** steel book mold setup, and **e** slab cast mold setup. **d** Al–10Ce ingot produced by book mold casting at a temperature of 800 °C with mold at room temperature, and **f** Al–10Ce ingot produced by slab casting at a temperature of 800 °C with mold at 400 °C

Results

Characterization of As-Cast Al–Ce Binary

Cast Al–Ce binary alloys with 10 and 16% Ce were produced with slab casting and their mechanical properties and microstructure was characterized. Figure 2a shows the mechanical properties (yield strength, tensile strength and elongation) of as-cast and heat-treated Al–10Ce and Al–16Ce alloy. It was determined that the eutectic composition exhibits the best performance (due to its fine microstructure), in agreement with previous reports in the literature. SEM micrographs are shown in Fig. 2b, c for the two compositions. SEM images confirm that the microstructure is eutectic and hypereutectic for Al–10Ce, and Al–16Ce, respectively. The fractographs of as-cast Al–10Ce and Al–16Ce are shown in Fig. 2d, e. The eutectic Al–10Ce showed the presence of dimples which indicates ductile failure (elongation at failure 13.44%), while Al–16Ce showed facets, which indicates brittle failure (elongation at failure 1.41%).

In a separate study, we produced Al–10Ce samples by the book mold method and compared their mechanical properties with those produced by slab mold casting, see Fig. 3. The figure includes data for the as-cast state and for samples that were heat-treated at 300 °C for 10 h and then tested at room temperature. The mechanical properties of slab cast specimens are superior to those of the book mold cast for both as-cast and annealed (300 °C, 10 h) states. An important observation is that the annealed samples lead to stress–strain curves very close to those of the as-cast samples. This demonstrates property retention after this type of heat treatment.

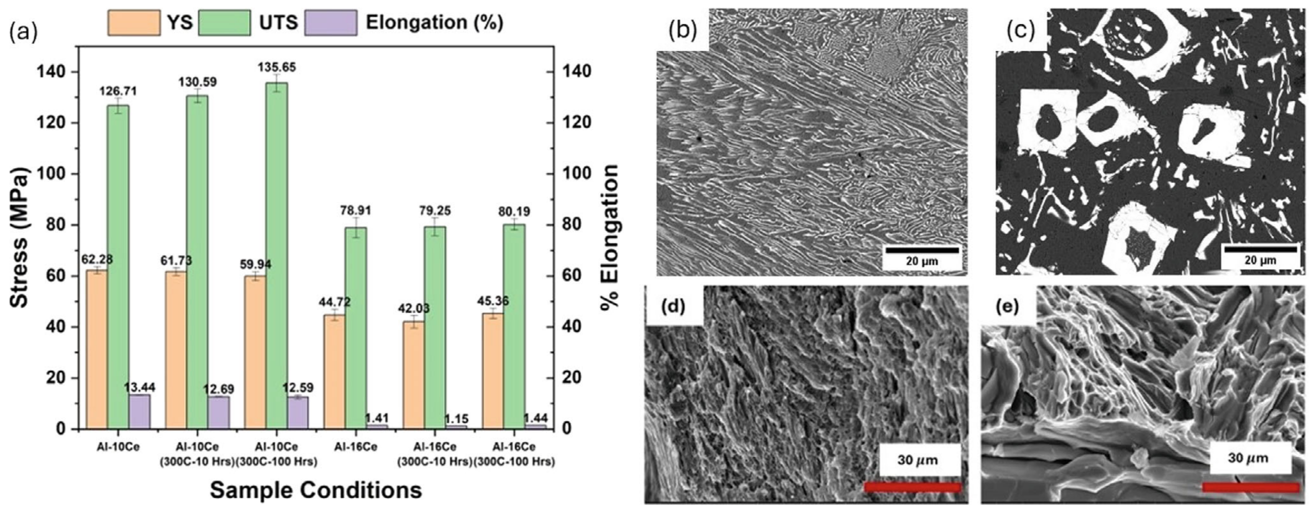

Fig. 2 **a** The yield strength, tensile strength and elongation of as-cast and heat-treated Al–10Ce and Al–16Ce alloy. Microstructure of as-cast **b** Al–10Ce alloy, and **c** Al–16Ce alloy obtained using slab cast mold. Images of the fracture surface are shown in **d** for the as-cast Al–10Ce alloy, and in **e** for the as-cast Al–16Ce alloy

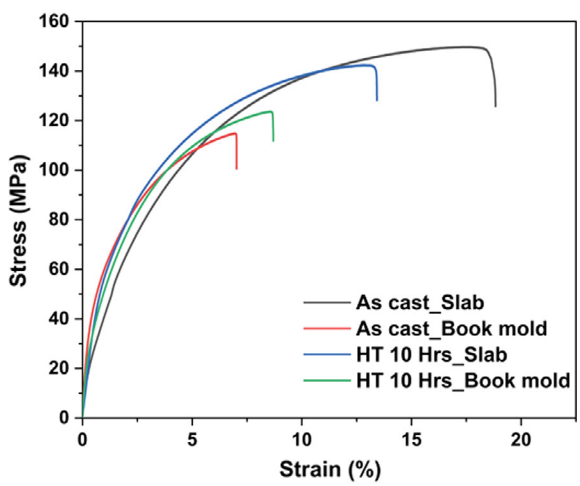

Fig. 3 Comparison of engineering stress–strain curves obtained with samples produced by the two casting methods (slab and book mold casting) for Al–10Ce alloy tested in as-cast and after exposure to 300 °C for 10 h

Characterization of the Extruded Al–10Ce Alloy

The microstructures of as-cast, extruded (86% area reduction), and annealed samples are shown in Fig. 4a–d. The extrusion process leads to a homogenous and refined microstructure. No significant differences are observed after annealing.

The XRD spectra of as-cast, extruded, and annealed samples are shown in Fig. 4e. The intensity of the [111] Al peak increases in the extruded samples, which dwarfs the other peaks of the spectrum. This indicates the development of texture during extrusion. Peaks corresponding to the $Al_{11}Ce_3$ phase are present in all cases, but become less visible in the extruded cases and on the scale of the figure. A slight change of texture is observed upon annealing.

Further, the effect on the microstructure and mechanical properties of the reduction in the extrusion process is explored by processing Al–10Ce at 86 and 93% area reduction. The microstructure and engineering stress–strain curves of the respective samples are shown in Fig. 5a–c. A finer microstructure is observed in the case of the 93% reduction. However, the tensile strength is higher in the case of the 86% reduction. Interestingly, the ductility of the material processed with the larger reduction is higher.

A comparison of the engineering stress–strain curves of extruded Al–10Ce and Al–16Ce is shown in Fig. 6a. The tensile strength of Al–10Ce and Al–16Ce samples in the extruded state is 95 and 127% larger relative to the as-cast states of the same materials (compare Fig. 6a with the data in Fig. 2a). The lower performance of the Al–16Ce is due to the presence of coarser brittle $Al_{11}Ce_3$ particles.

Tests are also performed at elevated temperatures of 150, 200, 250, 300, and 350 °C for as-cast and extruded Al–10Ce. The ratio of the UTS measured at temperature to the room temperature UTS, i.e. UTS_T/UTS_{RT}, is shown in Fig. 6b for as-cast and extruded states. Data for pure Al and several commercial Al alloys is also shown. The present alloys (both as-cast and extruded) show excellent thermal stability at all tested temperatures, with residual strength after annealing much larger than that of commercial alloys. This is due to the low diffusivity of Ce in Al which prevents microstructural coarsening. This is opposed to the situation of most commercial alloys in which precipitates dissolve at temperatures between 150 and 250 °C.

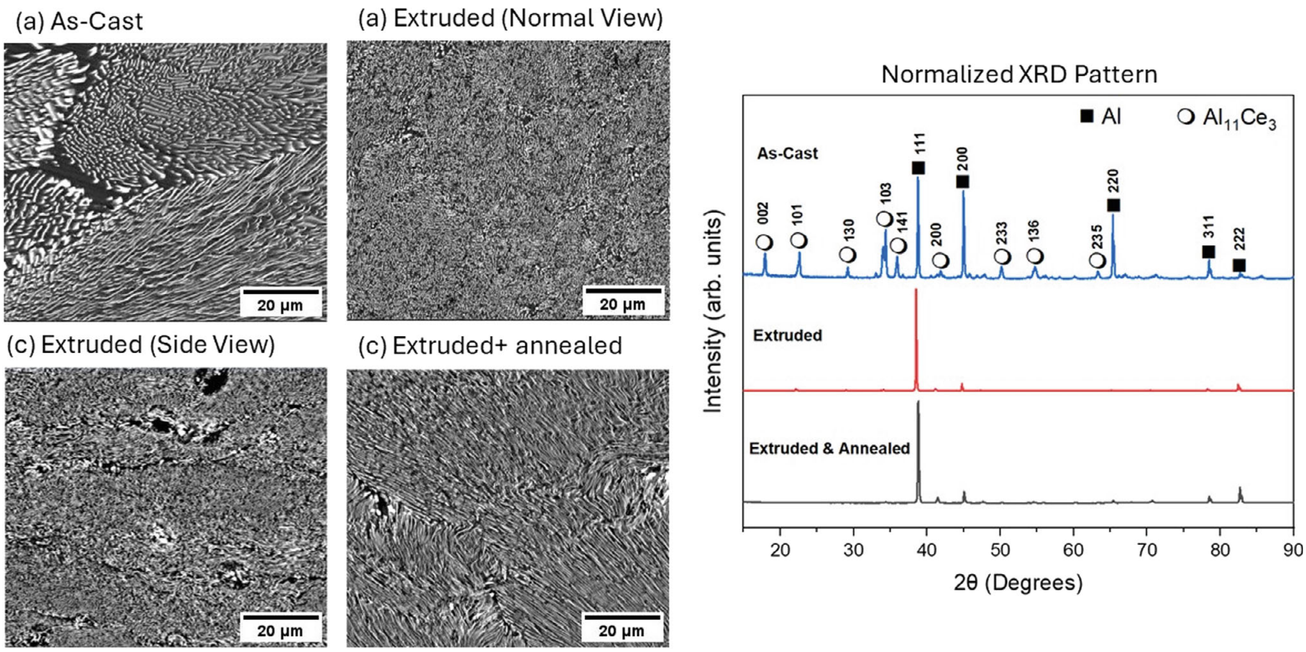

Fig. 4 The microstructure of Al–10Ce **a** as-cast sample, **b** extruded (normal view), **c** extruded (side view), **d** extruded and aged condition (normal view), **e** XRD of as-cast, extruded, and aged Al–10Ce

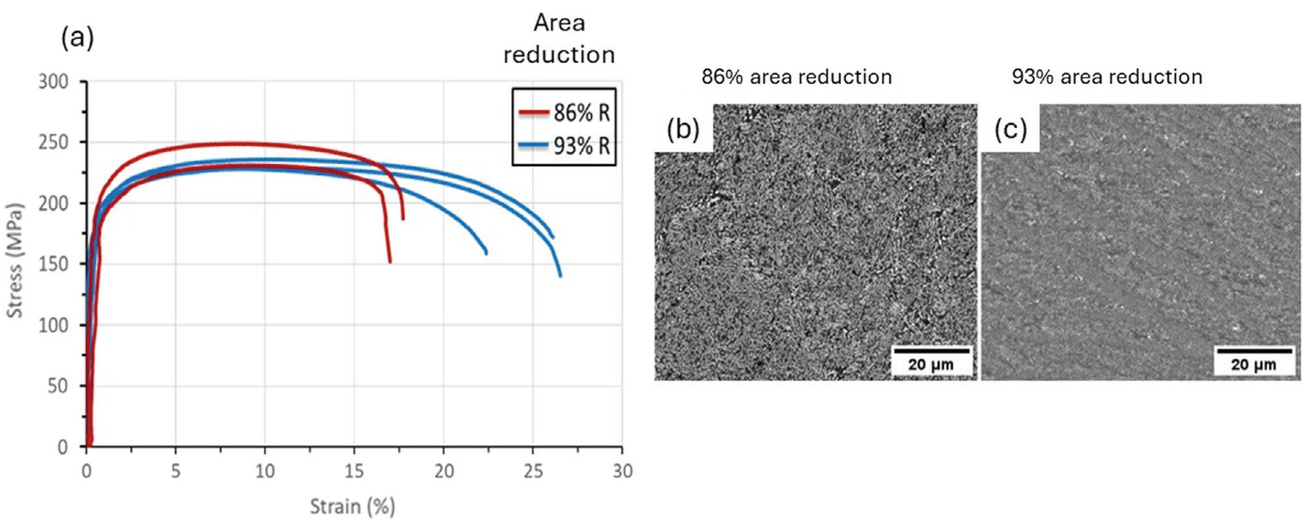

Fig. 5 **a** Engineering stress–strain curves of extruded Al–10Ce processed with area reductions of 86 and 93%. The microstructures of samples processed with 86 and 93% reduction are shown in (**b**) and (**c**), respectively

Microstructure Evolution of Al–10Ce upon Annealing for Extended Durations

Microstructural stability upon exposure to 300 °C for longer times (200, 300, and 400 h) was further evaluated. Figure 7 shows microstructures of as-extruded samples annealed at 300 °C for 200 h (Fig. 7a), 300 h (Fig. 7b), and 400 h (Fig. 7c). The larger precipitates break into fine and uniform particles during the extrusion process, and this structure is maintained after exposure to 300 °C for up to 400 h. The small diffusivity of Ce in Al inhibits precipitate coarsening. The fragmented precipitates are aligned in the extrusion direction (Fig. 4c).

The microhardness of samples annealed up to 400 h is shown in Fig. 7d. The hardness is largely insensitive to annealing, within the accuracy of the present measurement. The mean Vickers hardness of the various material states is shown in Fig. 7d. The XRD spectra for samples annealed up

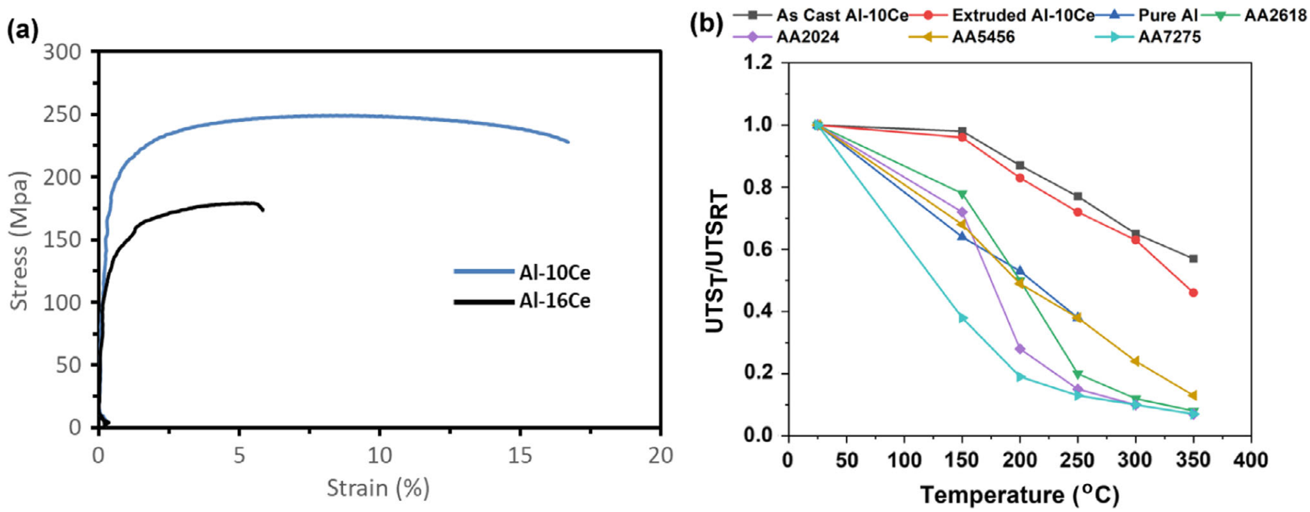

Fig. 6 **a** Engineering stress–strain curves of extruded Al–10Ce and Al–16Ce, and **b** comparisons of the ratio of the strength measured at temperature to the room temperature strength, UTS_T/UTS_{RT}, of present alloys with pure Al and several commercial high-temperature Al alloys

to 400 h at 300 °C are shown in Fig. 7e. The data indicates essentially no dependence on the annealing time and the presence of both Al(FCC) and $Al_{11}Ce_3$ phases in all material states.

EBSD Analysis and Modelling

Figure 8 shows results from EBSD analysis of Al–10Ce samples extruded and exposed to 300 °C for 10 h. Figure 8a shows the grain misorientation map, while Fig. 8b shows the KAM map. The fraction of grain boundaries with misorientation from 2 to 5° is 11%, those with misorientation between 5 and 15° represent 24%, and larger misorientations represent 65% of all boundaries investigated. The KAM map is indicative of the microstrain, which is almost negligible here as shown in Fig. 8b. It is likely that the residual stress introduced by processing is relaxed during heat treatment.

A section of the EBSD image was digitized and a finite element model of the microstructure was constructed. The Al grains are modeled as an elastic material with the Al anisotropic elastic constants and orientation indicated by the map in Fig. 8c. Three representations are selected for the $Al_{11}Ce_3$ particles in separate models (intermetallic particles and their crystallographic orientation are shown in Fig. 8d for the area approximately corresponding to Fig. 8c): the intermetallic precipitates are considered either rigid (Model I), isotropic with Young's modulus of 103 MPa and Poisson ratio $\nu = 0.3$ (Model II), and are transformed into pure Al grains in Model III (this model represents a pure Al sample). The elastic constants considered in Model II are computed as the isotropic version of the anisotropic intermetallic; the full elasticity tensor of the intermetallic used for the evaluation of the equivalent isotropic stiffness is taken from the literature [21]. These model microstructures are loaded in uniaxial tension, as shown in Fig. 8c, and the stress and strain fields are evaluated. Figure 9 shows the normal strain in the loading direction in the microstructure for the three models. The histograms of the normal strain values for the three models are shown in Fig. 9d. The strain distributions of Models II and III are identical, while the distribution of Model I has a heavy tail on the large strain end. This implies that considering the actual elasticity of the intermetallic particles does not lead to stress concentrations stronger than that present in the pure Al microstructure. This analysis indicates that the stiffness contrast between intermetallics and the Al surrounding is rather weak and should play no role in promoting plasticity or reducing fatigue life. It must be noted that other mechanisms associated with the presence of intermetallics may affect these mechanical properties.

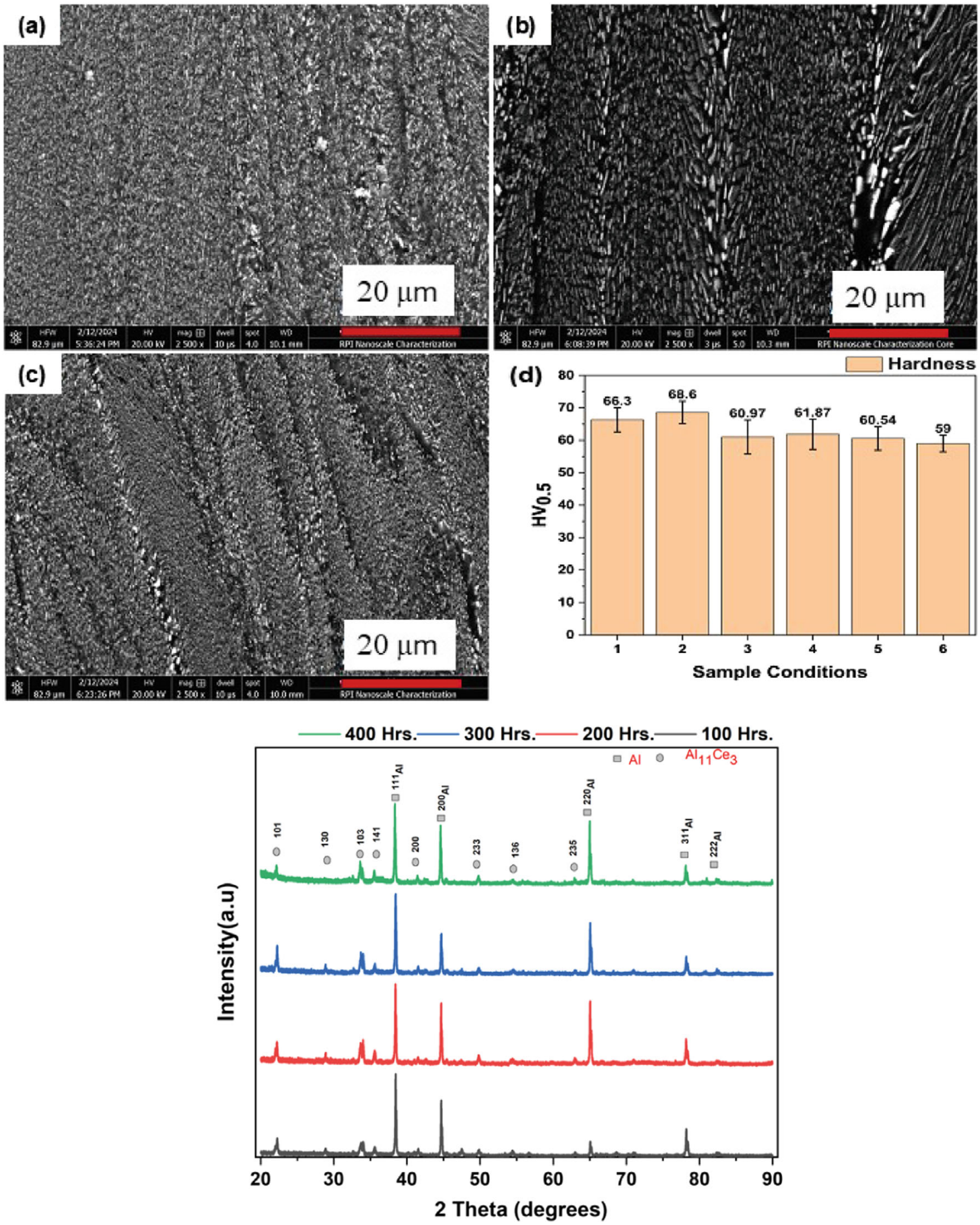

Fig. 7 The microstructure of extruded Al–10Ce samples annealed at 300 °C for **a** 200 h, **b** 300 h, and **c** 400 h. **d** Vickers hardness measured at room temperature for the same set of samples. The states indicated on the horizontal axis of the figure are 1—no annealing, 2—10 h, 3—100 h, 4—200 h, 5—300 h, and 6—400 h, all annealings being performed at 300 °C. **e** XRD pattern for 100, 200, 300, and 400 h anneals

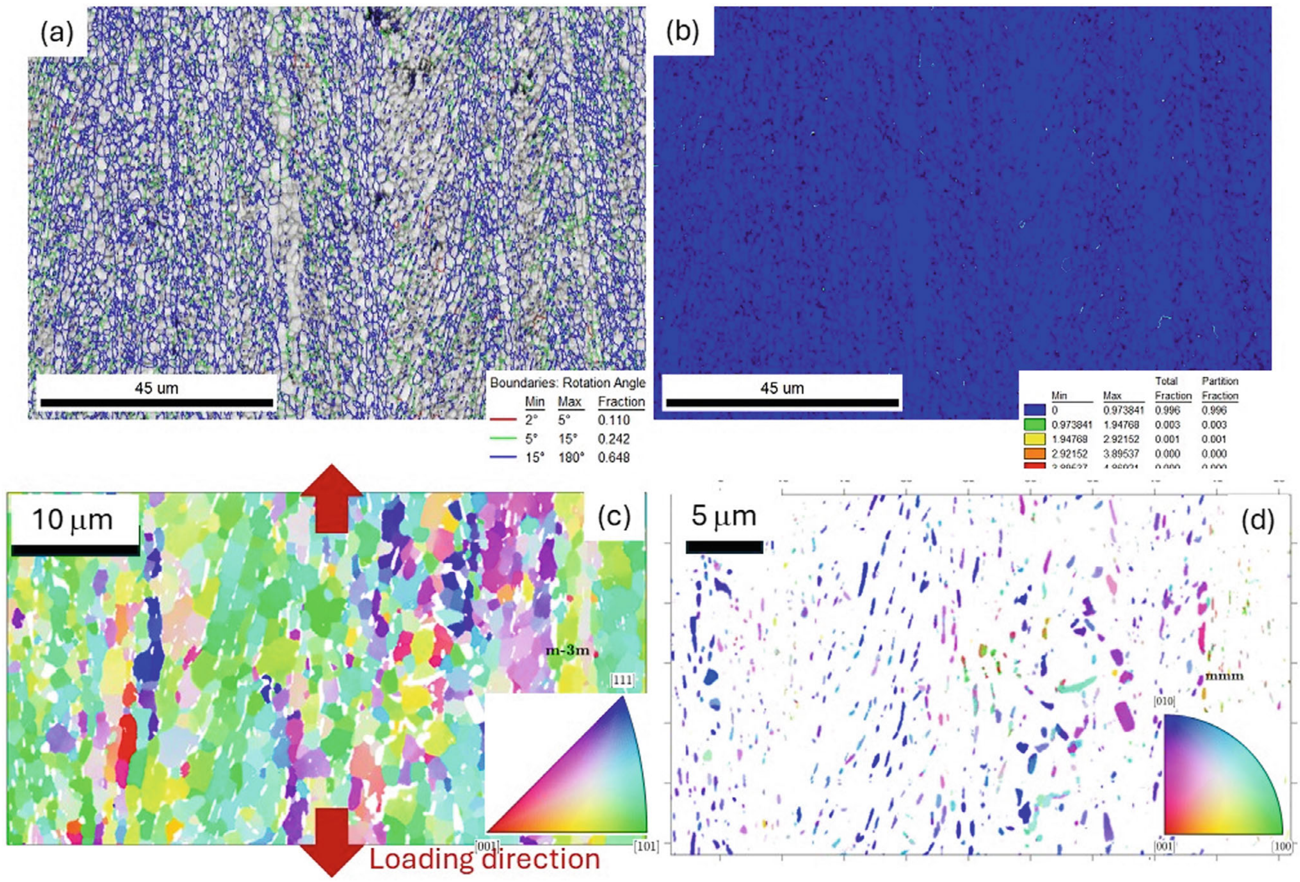

Fig. 8 **a** Grain misorientation map and **b** KAM map of Al–10Ce binary extruded and exposed at 300 °C for 10 h, **c** segment of the EBSD image of the same sample used as input to the model. The arrows indicate the direction of loading applied in the model. **d** $Al_{11}Ce_3$ intermetallic particles in the same sample

Conclusion

This study focuses on the effect of casting and extrusion on the structure, mechanical properties and thermal stability of Al–Ce binary alloys. In the as-cast state, the eutectic composition (Al–10Ce) exhibits the best performance (higher strength and ductility) due to its fine microstructure, in agreement with previous reports in the literature. Annealing the as-cast materials does not change the microstructure or mechanical properties. The slab cast alloys exhibited superior mechanical properties compared to the book mold castings in this study, but casting conditions were not well controlled or quantified and no conclusions can be drawn from this finding. Extrusion produces substantial microstructural refinement, i.e. both Al (FCC) grain size reduction and refinement of the $Al_{11}Ce_3$ intermetallic particles. The extruded materials have much larger strength and ductility compared with the as-cast state. As with as-cast, the extruded materials retain their mechanical properties upon annealing at 300 °C for durations up to 400 h, demonstrating outstanding thermal stability. This also indicates that adequate processing leading to microstructural refinement may render this class of alloys useful in applications in which high-temperature resistance along with excellent ductility are required.

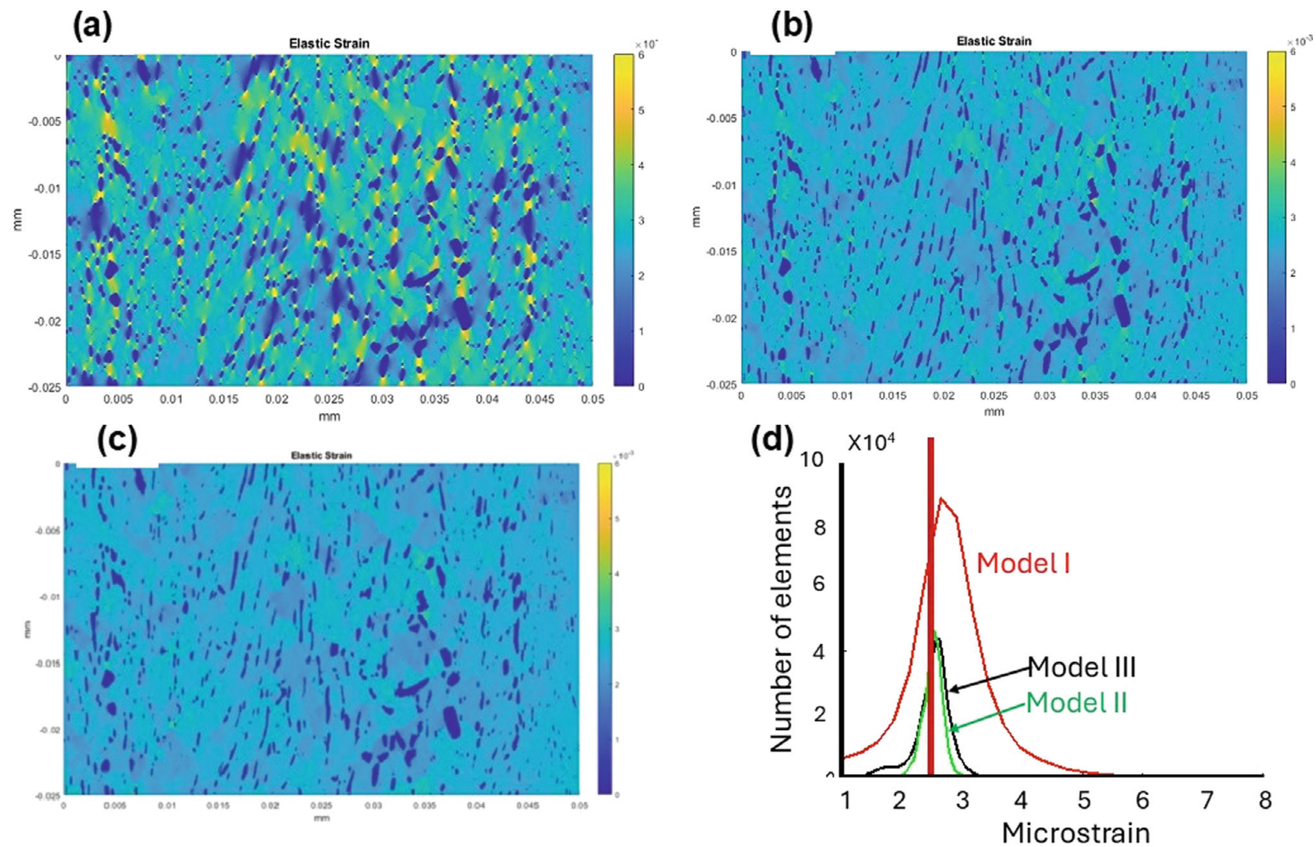

Fig. 9 Distribution of elastic strains from **a** Model I, **b** Model II, and **c** Model III. Histograms of the normal strain in the loading direction in the microstructures of panels (**a**)–(**c**) are shown in (**d**)

References

1. Y.H. Gao, C. Yang, J.Y. Zhang, L.F. Cao, G. Liu, J. Sun, E. Ma, Stabilizing nanoprecipitates in Al-Cu alloys for creep resistance at 300°C, Mater Res Lett 7 (2019) 18–25. https://doi.org/10.1080/21663831.2018.1546773.
2. F. Czerwinski, Thermal stability of aluminum–cerium binary alloys containing the Al–Al11Ce3 eutectic, Materials Science and Engineering: A 809 (2021). https://doi.org/10.1016/j.msea.2021.140973.
3. W. Wang, Q. Pan, G. Lin, X. Wang, Y. Sun, X. Wang, J. Ye, Y. Sun, Y. Yu, F. Jiang, J. Li, Y. Liu, Microstructure and properties of novel Al-Ce-Sc, Al-Ce-Y, Al-Ce-Zr and Al-Ce-Sc-Y alloy conductors processed by die casting, hot extrusion and cold drawing, J Mater Sci Technol 58 (2020) 155–170. https://doi.org/10.1016/j.jmst.2020.03.073.
4. A.E. Perrin, R.A. Michi, D.N. Leonard, K.D. Sisco, A. J. Plotkowski, A. Shyam, J.D. Poplawsky, L.F. Allard, Y. Yang, Effect of Mn on eutectic phase equilibria in Al-rich Al–Ce–Ni alloys, J Alloys Compd 965 (2023). https://doi.org/10.1016/j.jallcom.2023.171455.
5. A.D. D'Souza, S.S. Rao, M.A. Herbert, Assessment of influence of process parameters on properties of friction stir welded Al-Ce-Si-Mg aluminium alloy, Mater Res Express 6 (2019). https://doi.org/10.1088/2053-1591/ab1aec.
6. E.E. Moore, P.E.A. Turchi, V. Lordi, D. Weiss, Z.C. Sims, H.B. Henderson, M.S. Kesler, O. Rios, S.K. McCall, A. Perron, Thermodynamic Modeling of the Al-Ce-Cu-Mg-Si System and Its Application to Aluminum-Cerium Alloy Design, J Phase Equilibria Diffus 41 (2020) 764–783. https://doi.org/10.1007/s11669-020-00852-y.
7. Z. Lü, C. hui Mao, J. Wang, Q. shi Liang, S. wang Ma, W. jing Wang, Formation of interfacial Al–Ce–Cu–W amorphous layers in aluminum matrix composite through thermally driven solid-state amorphization, International Journal of Minerals, Metallurgy and Materials 27 (2020) 970–979. https://doi.org/10.1007/s12613-019-1952-0.
8. Y. Guo, J. Hu, Q. Han, B. Sun, J. Wang, C. Liu, Microstructure diversity dominated by the interplay between primary intermetallics and eutectics for Al–Ce heat-resistant alloys, J Alloys Compd 899 (2022). https://doi.org/10.1016/j.jallcom.2021.162914.
9. C. Zhang, P. Peng, H. Gao, Y. Wang, J. Wang, B. Sun, The important role of extremely low content of soluted Ce in the wide stacking faults formation in Al-Ce alloy, Scr Mater 214 (2022). https://doi.org/10.1016/j.scriptamat.2022.114647.
10. F. Czerwinski, Cerium in aluminum alloys, Journal of Materials Science 2019 55:1 55 (2019) 24–72. https://doi.org/10.1007/S10853-019-03892-Z.
11. F. Czerwinski, The Growth of Quaternary Divorced Eutectic in Al–Ce–Si–Mg Alloys, Metall Mater Trans A Phys Metall Mater Sci 54 (2023) 391–398. https://doi.org/10.1007/s11661-022-06911-y.
12. H. Okamoto, Al-Ce (Aluminum-Cerium), J Phase Equilibria Diffus 32 (2011) 392–393.

13. Y. Sun, C. Hung, R.J. Hebert, C. Fennessy, S. Tulyani, M. Aindow, Eutectic microstructures in dilute Al-Ce and Al-Co alloys, Mater Charact 154 (2019) 269–276. https://doi.org/10.1016/j.matchar.2019.06.010.
14. S. Shen, C. Wu, Y. Li, Y. Huang, W. Huang, P. Zhang, S. Zhong, Y. Lu, G. Luo, Z. Gan, J. Liu, Refining mechanism and elevated-temperature mechanical properties of Al-Ce alloys solidified under super gravity field, Materials Science and Engineering: A 879 (2023). https://doi.org/10.1016/j.msea.2023.145191.
15. D. Weiss, Improved High-Temperature Aluminum Alloys Containing Cerium, J Mater Eng Perform 28 (2019) 1903–1908. https://doi.org/10.1007/s11665-019-3884-2.
16. C. Zhang, Y. Wang, H. Lv, H. Gao, J. Wang, B. Sun, Enhanced load transfer and ductility in Al–9Ce alloy through heterogeneous lamellar microstructure design by cold rolling and annealing, Materials Science and Engineering: A 821 (2021). https://doi.org/10.1016/j.msea.2021.141591.
17. S.O. Rogachev, E.A. Naumova, E.A. Lukina, A. V. Zavodov, V. M. Khatkevich, High strength al–la, al–ce, and al–ni eutectic aluminum alloys obtained by high-pressure torsion, Materials 14 (2021). https://doi.org/10.3390/ma14216404.
18. S.O. Rogachev, E.A. Naumova, Thermal Stability of Al-Ca and Al-Ce Alloys Obtained by High-Pressure Torsion, J Mater Eng Perform 30 (2021) 9192–9199. https://doi.org/10.1007/s11665-021-06105-4.
19. A. E8/E8M, Standard Test Methods for Tension Testing of Metallic Materials, ASTM International (2013).
20. A. E384-17, Standard Test Method for Microindentation Hardness of Materials, (2016). https://doi.org/10.1520/E0384-17.
21. W.-J. Ding, J.-X. Yi, P. Chen, D.-L. Li, L.-M. Peng, B.-Y. Tang, Elastic properties and electronic structures of typical Al–Ce structures from first-principles calculations, Solid State Sci 14 (2012) 555–561. https://doi.org/10.1016/j.solidstatesciences.2012.02.006